Geochemical portray of the Pacific Ridge: New isotopic data and statistical techniques

Cédric Hamelin[a, *], Laure Dosso[b], Barry B. Hanan[c], Manuel Moreira[d], Andrew P. Kositsky[e] & Marion Y. Thomas[e]

[a] I.U.E.M., U.B.O., Place Nicolas Copernic, 29280 Plouzané, France
[b] Centre National de la Recherche Scientifique, UMR 6538, IFREMER, BP70, 29280 Plouzané, France
[c] Department of Geological Sciences, S.D.S.U., 5500 Campanile Drive, San Diego, CA 92182-1020, USA
[d] Institut de Physique du Globe de Paris, CNRS UMR 7154, 1 rue Jussieu, 75252 Paris CEDEX 05, France
[e] Tectonics Observatory, California Institute of Technology, Pasadena, CA 91125, USA

* Corresponding author : Cédric Hamelin, I.P.G.P, 1 rue Jussieu, Bureau 345, 75252 Paris CEDEX 05, France. Tel.: +33 1 83 95 76 72; fax: +33 1 7193 7710, email address : hamelin@ipgp.fr

ABSTRACT:
Samples collected during the PACANTARCTIC 2 cruise fill a sampling gap from 53° to 41° S along the Pacific Antarctic Ridge (PAR). Analysis of Sr, Nd, Pb, Hf, and He isotope compositions of these new samples is shown together with published data from 66°S to 53°S and from the EPR. The recent advance in analytical mass spectrometry techniques generates a spectacular increase in the number of multidimensional isotopic data for oceanic basalts. Working with such multidimensional datasets generates a new approach for the data interpretation, preferably based on statistical analysis techniques.

Principal Component Analysis (PCA) is a powerful mathematical tool to study this type of datasets. The purpose of PCA is to reduce the number of dimensions by keeping only those characteristics that contribute most to its variance. Using this technique, it becomes possible to have a statistical picture of the geochemical variations along the entire Pacific Ridge from 70°S to 10°S. The incomplete sampling of the ridge led previously to the identification of a large-scale division of the south Pacific mantle at the latitude of Easter Island. The PCA method applied here to the completed dataset reveals a different geochemical profile. Along the Pacific Ridge, a large-scale bell-shaped variation with an extremum at about 38°S of latitude is interpreted as a progressive change in the geochemical characteristics of the depleted matrix of the mantle. This Pacific Isotopic Bump (PIB) is also noticeable in the He isotopic ratio along-axis variation. The linear correlation observed between He and heavy radiogenic isotopes, together with the result of the PCA calculation, suggests that the large-scale variation is unrelated to the plume–ridge interactions in the area and should rather be attributed to the partial melting of a marble-cake assemblage.

Research Highlights

New Sr, Nd, Pb, Hf, and He isotopes data fill a sampling gap along the Pacific Ridge. ► We examine geochemical variation in MORB using a principal component analysis. ► A progressive change in the depleted matrix is recognized along the Pacific ridge. ► In samples devoid of plume influence, He isotopes correlates with Pb isotopes.

Keywords: oceanic basalts; Pacific–Antarctic Ridge; mantle heterogeneity; Principal Component Analysis; Sr Nd Pb Hf isotopes

1. Introduction

Mid-oceanic ridge basalts (MORB) are the result of continuous melting of the ambient upper mantle beneath oceanic ridges. The MORB-source mantle is generally thought to have been depleted ~2 Gy ago by extraction of the continents. Although the range of geochemical variations in oceanic basalts is mostly attributed to the influence of Ocean Island Basalt (OIB), significant geochemical heterogeneity in MORB has been recognized (Hoffman et al., 2003 and reference therein; Rudge et al., 2005). This heterogeneity has been revealed using radiogenic isotope ratios (Sr, Nd, Pb and Hf) in areas devoid of plume influence. Numerous studies have attempted to model the mixing relationship between enriched and depleted domains within the mantle to reproduce the range of isotopic variations observed in oceanic basalts (Albarède, 2001; Meibom and Anderson, 2004; Rudge et al., 2005; Kellogg et al., 2007). The range of Sr, Nd and Pb isotopic compositions depends not only on the end-member compositions but also on the volume of mantle sampled during the melting relative to the length scale of heterogeneities (Kellogg et al., 2007). Therefore, the range of MORB geochemical variations reflects the size, the spatial distribution, and the difference of fusibility of heterogeneities within the upper mantle. In addition to this intrinsic heterogeneity of the MORB mantle, radiogenic isotope studies have led to the definition of distinct broad mantle isotopic domains, such as the archetypal DUPAL anomaly located in the south hemisphere (Dupré and Allègre, 1983; Castillo, 1988). Boundaries between these domains can be (i) extremely sharp as seen at the Antarctic Australian–Antarctic Discordance (ADD), with isotopic ratios (Sr, Nd, Pb and Hf) abruptly changing from Indian to Pacific values (Pyle et al., 1992, Hanan et al., 2004; Meyzen et al., 2007; Cooper et al., 2009) or (ii) more gradual as seen in the transition from Southwest Indian Ridge to South Atlantic MORB (Meyzen et al, 2005).

Another example of these large geochemical provinces is given by the two sub-pacific mantle domains (Vlastélic et al., 1999). The distinctive isotopic properties of these large-scale geochemical domains suggest a long-term isolation of these mantle provinces, each with their own convective histories involving various amounts of melting residues and recycled components. On the basis of an incomplete dataset, a boundary between these two pacific provinces has been located at the latitude of the Easter Island microplate (Vlastélic et al., 1999). But in order to have a complete geochemical view of the southern Pacific Ridge from 66 to 10°S, it was necessary to fill the sampling gap between 53°S and 41°S. This became one of the main objectives of the PACANTARCTIC2 cruise which took place in 2004-05 (Dosso et al. 2005, Klingelhoefer et al., 2006, Moreira et al., 2008; Hamelin et al., 2010). Analyses of Sr, Nd, Pb, Hf and He isotopic compositions of these new samples from the Pacific Antarctic Ridge (PAR) are compiled here together with published data from 66°S to 53°S and from the East Pacific Rise (EPR). Therefore it becomes possible to have a picture of the geochemical variations along the entire Pacific Ridge from 66°S to the 10°S. Adapting a Principal Component Analysis (PCA) to incomplete datasets, we show a detailed portray of the geochemical variability of the Pacific Ridge.

2. Data selection and analytical methods.

2.1. The Pacific Ridge database from 10 to 66°S.

Along the Pacific Ridge, the Chile Triple Junction at 35°S/110°W separates the PAR from the EPR. The two pacific ridges show different geological settings: the full spreading rate increases along the PAR from 54 mm/yr at 65°S to 100 mm/yr at 35°S whereas it decreases along the EPR from 158 mm/yr at 35°S to 146 mm/yr at 10°S. In conjunction, the ridge axis morphology changes from a valley to a dome north of 60°S along the PAR (Ondréas et al.,

2001), whereas the EPR is characterized by a uniform dome shaped morphology. Three plume-ridge interactions generate abnormal morphological structures along this section: Foundation (~38°S), Easter Island (~26°S) and 17°S. They are recognized by a high ridge cross-sectional area (Klingelhöfer et al., 2006) and the presence of intense off-axis volcanic activity. Compared to the EPR, the Pacific Antarctic Ridge still remains geochemically poorly known. A large portion of this plate boundary has been previously surveyed (Lonsdale, 1994; Cande et al., 1995) but the northern part has only recently been sampled (Dosso et al., 2005; Moreira et al., 2008; Hamelin et al., 2010).

To generate a coherent database along the pacific ridges, on-axis samples analyzed for one or more isotopic ratios (Sr-Nd-Pb-Hf-He) are selected from 66°S to 10°S using our new isotope data (table 1) completed with the petrological database of the Lamont-Doherty Earth Observatory (http://www.petdb.org). In most cases when the reference values of the standards are reported, the data are normalized to the values of NBS987, 0.71025 for Sr, of JNdi-1, 0.512104 and La Jolla, 0.511852 for Nd, NBS981, $^{206}Pb/^{204}Pb$=16.9373, $^{207}Pb/^{204}Pb$=15.4925, $^{208}Pb/^{204}Pb$=36.7054, for Pb and JMC475, 0.282162 for Hf (see http://georem.mpch-mainz.gwdg.de/ for details and references).:

2.2. Analytical methods.

2.2.1. Double Spike Pb analyses along the PAR

New high-resolution Pb analyses were carried out for samples collected during PACANTARCTIC1 (PAC1) and PACANTARCTIC2 (PAC2) cruises along PAR segments from 66°S to 56°S and from 53°S to 41°S respectively (Fig. 1, Table 1). Small chips from the inner part of the pillow lavas were handpicked to avoid altered surfaces that could be a potential source of Pb contamination. Powdered samples were leached with 6M HCl at 140°C

for an hour and then rinsed up to 6 times with ultrapure water prior to dissolution. Lead separation was then performed on an anionic exchange resin. Pb analyses were performed at Ifremer (Centre de Brest) on a Finnigan MAT 26x multicollector instrument (MAT261 upgraded by Spectromat), using the double spike technique with the calibrated Southampton-Brest 207/204 spike (Ishizuka et al., 2003). Replicate analyses of the Pb isotope standard NBS981 gave an average of 16.9432±0.0027 and 15.5004±0.0029 and 36.7326±0.0086 for $^{206}Pb/^{204}Pb$, $^{207}Pb/^{204}Pb$ and $^{208}Pb/^{204}Pb$, respectively. Pb blanks measured using this procedure were < 100 pg, and thus negligible relative to the amount of sample analyzed.

2.2.2. Hf measurements along the PAR

Hafnium isotopic compositions were analyzed along the PAC1 ridge segments at SDSU on splits from the same samples (Hamelin et al., 2010). Hf was separated using the protocol of Blichert-Toft et al. 1997 with a negligible blank of less than 25 pg. Hf isotope ratios were measured at SDSU using the Nu Plasma. The $^{176}Hf/^{177}Hf$ was normalized for mass fractionation relative to $^{179}Hf/^{177}Hf$=0.7325. The JMC-475 Hf standard $^{176}Hf/^{177}Hf$ gave 0.282160 ±0.000010 (2σ) during this study. The standard was run alternately with samples to monitor machine performance.

2.2.3. He measurements along the PAR

Helium isotopic compositions have been measured on PAC1 and PAC2 samples at IPGP (Institut de Physique du Globe de Paris). Fresh pieces of glass were cleaned with distilled water, ethanol and acetone using an ultrasonic bath. Some samples were also cleaned with hydrogen peroxide in order to remove some Mg crust. Analytical procedure is identical to previous studies from our laboratory and can be found in Moreira et al. (1995). Samples were crushed under vacuum with analytical blanks of 7±1 nccSTP ^{4}He. This corresponds to 0.02 to

0.4% of the samples. Helium concentrations and isotopic composition were measured using the ARESIBOII mass spectrometer (Moreira et al., 2008).

3. New results compared to published MORB data along this ridge section.

These results include samples from 66°S to 56°S (PAC1) and from 53°S to 41°S (PAC2) (Fig. 1). New high resolution Pb analyses as well as Hf and He analyses are presented here in Table 1. The Sr, Nd and Hf analyses on the same samples are found in Vlastélic et al. (2000) and Hamelin et al. (2010).

3.1. Binary isotopic correlations

With 7 isotopic ratios, the number of possible binary isotope diagrams is 21. As an example, we choose here to describe 4 such binary plots, selecting some of the most commonly discussed (Fig. 2A-D). In all diagrams, pacific MORB samples devoid of plume influence define linear correlations that in most cases have been previously described in the literature. This result is in good agreement with the expected coherence in behavior between Rb-Sr, U-Pb, Th-Pb, Sm-Nd and Lu-Hf isotopic systems compared to each other during magmatic processes. When plume-ridge interaction samples are included in our dataset, they define elongated fields overlapping PAR-EPR array except in Figure 2C where He-ε_{Nd} isotopic ratios define sub-parallel trends which emerge from the PAR-EPR array and point towards higher $^{3}He/^{4}He$ (R/Ra) ratios. More than 30 years of He isotopes systematic of oceanic basalts worldwide have shown that MORB samples are characterized by a narrow

range of composition compared to OIB samples. However even within this limited range, our data show a linear correlation between $^{3}He/^{4}He$ (R/Ra) values and ε_{Nd} (Fig. 2C). The correlation between He and other isotopic systems will be discussed further below (§4.4.2).

In contrast with the decoupling of Hf and Nd isotope compositions previously documented in MORB (e.g., Patchett and Tatsumoto, 1980; Salters and White, 1998; Chauvel et al., 2001; Debaille et al., 2006), a rather good correlation between these two isotopic systems is observed along our studied are (Fig. 2B). Debaille et al. (2006) have suggested that a distinctive behavior of Hf during disequilibrium melting along their studied ride area (Atlantic ridge 22-35°N) could explain a decoupled behavior of $^{176}Hf/^{177}Hf$ with respect to other isotopic ratios. The linear correlations observed in our dataset, show that the hypothesis of a specific behavior of Hf does not apply along the pacific ridges. Recently, good correlations between Hf and Nd isotopic ratios have been reported from other ridge segments such as Mohns Ridge (Blichert-Toft et al., 2005) and the entire mid-Atlantic Ridge (Agranier et al., 2005).

3.2. MORB variability along the south Pacific Ridge.

Latitudinal isotopic variations of south Pacific Ridge basalts are shown in Figure 3. An important geochemical feature from 66 to 10°S is a large scale (spanning approximately 5000km) and coherent variation of all isotopes shown by a bell shape grey line. The extremum of this variation defining the Pacific Isotopic Bump (PIB), is located at the latitude of Foundation (38°S). It reveals a less depleted component, characterized by more radiogenic values for Sr, Pb isotopic ratios, and correlatively less radiogenic values for Nd and Hf. Three shorter wavelength variations of the order of 200 to 700km are seen as isotopic anomalies superimposed on the otherwise bell shaped curve of the isotope signature along the ridge. In a way similar to the Pacific Isotopic Bump, these variations are towards more radiogenic Sr and

Pb values and coherently less radiogenic Nd and Hf values. They indicate the influence of enriched materials due to plume-ridge interactions.

Helium isotopes do not fit this Sr-Pb/Hf-Nd coherent behavior. At the latitude of the Foundation-Ridge intersection (38°S), the bell-shaped He curve shows radiogenic $^{3}He/^{4}He$ ratios. But on the other hand, hot-spot influenced samples form negative "plume anomalies" with very unradiogenic signatures (high $^{3}He/^{4}He$ ratios, up to 12 R/Ra). The amplitudes of the PIB and the anomalies attributed to the plume effect are of the same order of magnitude for Nd, Hf and Pb. For He and Sr, the PIB has much smaller amplitude than the hotspot anomalies. Additionally, local MORB variability is expressed as spikes, which are likely related to transform faults (Eltanin System).

4. Discussion

4.1 Statistical definition of mantle reference lines

In most binary plots of radiogenic isotopic ratios, representative points of mantle derived material define linear trends. Historically, these trends have been used to define reference lines such as the Northern Hemisphere Reference Line (NHRL) in Pb-Pb plot (Hart, 1984) or the "Mantle Array" in Sr-Nd plot (DePaolo and Wasserburg, 1979) and the Nd-Hf plot (Vervoort and Blichert-Toft, 1999). These reference lines are arbitrary and depend on the abundance of data available at the time of their definition. However, the data colinearity in these plots justifies these convenient choices. The NHRL has been convenient to quantify the Dupal anomaly using the $\Delta 7/4$ and $\Delta 8/4$ (Hart, 1984). In 1999, new MORB data from the south Pacific lead to the definition of the Pacific Reference Line (PRL) which proved convenient to compare two sub-pacific mantle domains, using the δ(Nd-Sr) and δ(Sr-Pb) notations (Vlastélic et al., 1999). With the recent advance in analytical MC-ICPMS

techniques, the number of isotopic data increases dramatically. It becomes possible to look at these reference lines in multidimensional space from a statistical point of view. Principal Component Analysis (PCA) is a powerful mathematical tool to study data sets such as a geochemical database including Sr-Nd-Pb-Hf analyses. The purpose of PCA analysis is to reduce the number of dimensions in a data set by keeping those characteristics that contribute most to its variance. This technique has been used in previous mantle heterogeneity studies (e.g. Agranier et al., 2005, Debaille et al., 2006) The PCA method used with our geochemical dataset has been initially developed for low-rank matrix approximations (Srebro and Jaakkola, 2003) and was recently adapted for tectonic problems using incomplete geodetic times series (Kositsky and Avouac, 2010). The main difference with traditional PCA methods is that the singular value decomposition is replaced by a more sophisticated decomposition, which appropriately takes into account samples with a missing isotope measurement. This technique is particularly suitable to geochemical data as it allows computing the principal components using the whole dataset, increasing therefore the accuracy of the calculation (see supplementary material for a more detailed discussion about the concept and the limits of our calculation). Although more recently ICA (Independent Component Analysis) has been chosen by some authors (Iwamori and Albarède, 2008, Iwamori et al., 2010), the preferred PCA method used here has the advantage of dealing with missing isotopic data, assuming that decorrelation is still a good assumption of independence in our dataset.

Because the PCA method is an orthogonal linear transformation, it assumes the linearity of the data co-variations. In most binary isotopic diagrams, mixing processes are expressed by hyperboles whose curvatures depend on the elemental concentration ratios of the involved end-members. But in the case of MORB, pseudo-linear correlations are observed (Fig. 2) indicating that denominator elements are in approximately constant proportions in the mixing components. It is very difficult to evaluate the extent of non-linear relationships concealed

239 within the analytical noise. However, it is worth noting that the geographical variations of the
240 components calculated with our method are approximately the same as those computed in the
241 3-dimensional space of Pb isotopes, in which relationships are linear. In order to minimize the
242 correlations induced by the ^{204}Pb analytical noise (it represents only about 1.4% of the total
243 Pb), the computation has been made in the $^{204}Pb/^{206}Pb$, $^{207}Pb/^{206}Pb$ and $^{208}Pb/^{206}Pb$ space.
244 Considering the problematic of our study, this observation suggests that the curvature can be
245 neglected. One drawback of PCA in general stems from the fact that PCA is a projection
246 method, and sometimes low-dimensional visualization can lead to erroneous interpretations.

247 ### *4.2. Distribution of the variance among the principal components.*

248 The most striking result of the PCA is that the first principal component accounts for more
249 than 70% of the total variance. This result is remarkable considering the number of
250 geochemical parameters involved in the very large number of samples used in this analysis. It
251 indicates the strong coherence of all isotopic ratios within the depleted mantle domain. These
252 correlations in binary plots of isotopic systems are the result of two antagonistic processes
253 that took place over time: chemical fractionation events leading to the existence of enriched
254 and depleted mantle reservoirs and mechanical mixing of theses reservoirs during mantle
255 convection. The chemical fractionation between parent and daughter isotopes is controlled by
256 distribution coefficients. Even if these coefficients can be modified by multiple parameters,
257 they remain consistent from one element to another. Since these processes are approximately
258 linear, the resulting dispersion is located along a line corresponding to PC1 (the first Principal
259 Component).

260 While the importance of the first component is indisputable, one challenge with PCA is to
261 establish the number of significant components needed to explain the observed data variance.
262 A classical way to illustrate the number of relevant components is to study the residual
263 variance (χ^2) obtained for each component (e.g. Kositsky and Avouac, 2010). This value

drops abruptly after the third component (see supplementary material). At first, we can infer that the information brought by the fourth to the sixth principal components is statistically insignificant and can safely be ignored. Using a PCA computed in the 3-dimensional space of Pb isotopes, the principal components account for 91.7%, 8.2% and 0.1% of the variance for PC1, PC2 and PC3 respectively. This observation suggests that the variance expressed by principal components over the order of 2 is the result of a randomly distributed error. Also the absence of coherent geographical variation for the third component suggests that this variance could either be a very local variation or an artifact of our data compilation (i.e. sampling bias, data and error normalization between different laboratories). This justifies to limit the discussion of the south pacific mantle heterogeneity to the PC1 and PC2 characteristics.

4.3. Mapping geochemical heterogeneities in the mantle using a PCA method.

Using the dataset available at the time, Vlastélic et al. (1999) identified a large geochemical variation in the south Pacific depleted mantle. Based on an incomplete sampling of the ridge, they suggested the existence of a sharp boundary located at the latitude of the Easter Island Microplate (27°S). As an interpretation, they proposed that the Pacific Superswell divided the mantle into two domains each with their own convective histories, producing slight differences in their average isotopic signatures. More recently, the origin of these two domains has been challenged by a model based on plate kinetics (Small and Danyushevsky, 2003). Small and Danyushevsky proposed that geochemical discontinuities result from variations of the asthenosphere consumption, which corresponds to the ratio between the accretion rate and the spreading center migration relative to plumes. Their model predicted that the fast spreading, slowly migrating East Pacific Rise should have higher average melting degrees compared to the slower spreading, rapidly migrating Pacific-Antarctic Rise. In order to identify the two mantle domains along the Pacific Ridge, Vlastélic

et al. (1999) used δ(Sr-Pb) and δ(Nd-Sr), which are defined as the vertical deviations from references lines in Pb vs Sr and Sr vs Nd isotopic ratio plots respectively. These reference lines (see §4.1) were drawn intuitively in the greatest variance of their dataset. They can be directly compared to our first principal component. By construction, whatever the number of dimensions considered in the PCA, the projection of PC1 in a binary diagram resembles the relevant reference line (Fig. 2). Because PC2 is orthogonal to the greatest variance, sample values along this component are correlated to delta notations such as δ(Sr-Pb), δ(Nd-Sr) or Δ8/4Pb. But compared to delta notations, PC2 has the advantage of being rigorously and statistically determined in a multidimensional isotopic space. The application of the PCA method to our data compilation (excluding He isotopes) reveals a geochemical profile of the Pacific Ridge. The plot of PC1 versus latitude summarizes all the characteristics noted with the different isotopic systems (Fig. 4). The short scale geochemical variations associated with hotspots as well as the large-scale variation are clearly visible. 17°S and 25°S (Easter Island) are well defined by sharp anomalies superimposed on the bell shaped curve. A plot of PC2 versus latitude shows a very different picture (Fig. 4): only the large scale variation is expressed by this component, the geochemical variations associated with hotspots are flattened and the corresponding samples are projected along the bell shape curve defining the Pacific Isotopic Bump. This PIB is also shown on plots of delta versus latitude, illustrating the equivalence of these parameters and PC2 (Fig. 4). At the Juan Fernandez/Foundation latitude (36°S), the isotopic variation curve reaches an extreme which corresponds to a less “depleted” isotopic signature. In contrast with the conclusion of Vlastélic et al. (1999), we proposed that geochemical variations along the Pacific Ridge are not the result of two separated mantle domains but should rather be seen as a progressive variation of the isotopic composition of the sub-Pacific depleted mantle. Since the asthenosphere consumption varies abruptly at the Chile triple junction and is almost constant along the PAR, the plate kinematic model of Small and

Danyushevsky (2003) is also inconsistent with the observed progressive variation of the MORB depleted matrix.

4.4. Mixing relationship within the depleted mantle compared to ridge-hotspot interactions.

4.4.1. Asthenospheric versus hotspots signals as illustrated by Sr-Nd-Pb-Hf.

Except in figures involving He isotopes, geochemical variations related to ridge/hotspot interactions are consistent with variations of samples devoid of plume influence. At first, it is difficult to distinguish the two types of variations in binary isotopic plots (Fig. 2). Nevertheless, a PCA computed with all heavy radiogenic isotopes clearly illustrate a difference: hotspot signatures are exclusively visible with PC1, while the variance related to the large scale variation (PIB) is illustrated by both PC1 and PC2 versus latitude (Fig. 4). In PC1 versus PC2 space, the MORB field extends from the depleted end member of the mantle (DMM) toward a recycled oceanic crust end member with a HIMU affinity (Fig. 5). The samples identified as resulting from a plume-ridge interaction are not part of this "depleted trend". Rather their data field extends from the depleted trend towards more enriched-type end members such as C and/or EM. This observation supports the idea that the large scale variation in the depleted Pacific mantle is unrelated to ridge/hotspot interactions. This variation is therefore equivalent to the intrinsic variability of MORB recognized in other areas (e.g. Dosso et al., 1999, Donnelly et al., 2004; Debaille et al., 2006; Hémond et al., 2006). It has to be noted that PCA calculations assume a linearity criteria which is not satisfied when dealing with isotopic compositions of the mantle end-members. It is thus not possible to determine more precisely the nature of the different mantle components responsible for the observed trends. Nevertheless, the PCA calculations establish that the progressive

338 geochemical change of the depleted matrix of the Pacific mantle is not the result of hotspot
339 material being diluted into the depleted mantle. Using a different approach, Meyzen et al.
340 (2007) successfully unscrambled the hotspot and asthenospheric signals. These authors have
341 proposed that the geochemical variations unrelated to ridge/hotspot interactions along the
342 South West Indian ridge and the South Atlantic ridge are related to a broad lower mantle
343 upwelling in this area. Similarly, a broad lower mantle input could be a plausible cause of the
344 Pacific Isotopic Bump associated with the high spreading rates in the vicinity of the Chile
345 Ridge Triple junction.

346 It is interesting to compare the results of our PCA calculation along the Pacific ridge with
347 the spectral analysis performed along the Atlantic ridge by Agranier et al. (2005). These
348 authors found two contrasting types of spectra along their study area. The first type is
349 associated with ridge-hotspot interactions and is seen in the first principal component. The
350 second type is illustrated by the continuous power decrease with the decreasing wavelength of
351 the second principal component. Agranier et al. (2005) have interpreted this second type of
352 spectra, unrelated to hotspots, as being the result of the continuous size reduction of mantle
353 heterogeneities upon stretching and refolding of the convecting mantle. Despite the
354 differences in geological settings between the Pacific ridge and the Atlantic ridge, our
355 observations are in good agreement with the statistical analysis of Agranier et al. (2005). We
356 view the PIB as the consequence of a progressive change in the relative proportions of the
357 marble-cake components present in the Pacific upper mantle. In this model, hotspot anomalies
358 are superimposed on the intrinsic mantle heterogeneity expressed in MORB.

359

360 *4.4.2. He isotopes in the depleted mantle compared to hotspot signals.*

361 Unlike other isotopic systems, helium shows a first order discrepancy between the hotspot
362 and the depleted mantle signals in our studied area (Fig. 3 and Fig. 6): the large scale variation

363 associated to the depleted mantle is characterized by an increase towards more radiogenic
364 (low $^{3}He/^{4}He$) compositions, whereas the short scale variation associated to the mantle plumes
365 points towards high $^{3}He/^{4}He$ values as previously noted in Hanan and Graham (1996). The
366 origin of the large range of elevated $^{3}He/^{4}He$ values in OIB lavas is a long-lived controversial
367 question (Kurz et al., 1982; Allègre et al., 1983; Meibom et al., 2003; Moreira et al., 2004).
368 Historically, the requirement of a high $^{3}He/^{4}He$ reservoir for the OIB lead to the idea that
369 plumes are tapping a deep, undegassed lower mantle, isolated from the upper mantle
370 convection (O'Nions et al., 1996; Allègre et al., 1997). Numerous alternative models have
371 tried to solve the apparent inconsistency between the high $^{3}He/^{4}He$ ratio in plumes and the
372 requirement of a source previously processed through partial melting (e.g. Parman et al.,
373 2005; Class and Goldstein, 2005; Purtika, 2008; Albarède, 2008; Davies, 2010).

374 Compared to plume-influenced samples, systematics of He isotopes in depleted MORB
375 samples have shown a very restricted range of $^{3}He/^{4}He$ with a peak of distribution around 8±1
376 (R/Ra) (Allègre et al., 1995). Within the uncontaminated depleted mantle sampled along our
377 studied area, $^{3}He/^{4}He$ varies from 6 to 9.5 (R/Ra). Samples devoid of plume influence fall
378 along a negative trend toward low $^{3}He/^{4}He$ values and high $^{206}Pb/^{204}Pb$. This variation of He
379 isotopes in our samples devoid of plume influence is clearly related to the PIB identified
380 along the pacific ridge using PCA with Sr, Nd, Pb and Hf isotopes. It is interesting to note
381 that the most enriched samples from this correlation show the lowest $^{3}He/^{4}He$ values (more
382 radiogenic). In order to reconcile the $^{3}He/^{4}He$ variations with variations of Sr, Pb, Nd and Hf
383 isotopes, new models take into account the physical specificities of He compared to heavy
384 radiogenic isotopes: its diffusivity in mantle conditions and its capacity to be outgassed from
385 melts at sub-surface pressure (e.g. Hart et al., 2008; Albarède et al., 2008; Gonnermann and
386 Mukhopadhyay, 2009). We propose that the melting of a marble-cake upper mantle,
387 unpolluted by plumes, produces the good correlation observed between He and Pb isotopes in

388 our depleted samples. The less depleted component of the mantle assemblage is characterized
389 by a high Pb isotopic ratio and a low $^{3}He/^{4}He$ ratio. We suggest that this component was
390 derived from the recycling of an extensively outgassed oceanic crust. When the oceanic crust
391 is subducted back into the mantle, it contains negligible concentration of mantle-derived He
392 (Staudacher and Allègre, 1988). With time, this very low $^{3}He/(U+Th)$ in subducted slabs is
393 expected to produce the end-member with high Pb isotopes value and low $^{3}He/^{4}He$ ratio (Fig.
394 6).
395 In our model, the variation of He isotopes along the pacific ridge could be interpreted as:
396 (1) a smaller contribution of the refractory layers (less radiogenic), corresponding to a lower
397 $^{3}He/^{4}He$ ratio at the PIB but because the melting rate is expected to be higher near the Chile
398 Ridge Triple Junction, this hypothesis seems very unlikely, or (2) a higher volume of the
399 recycled end-member in this area. This hypothesis is in agreement with the conclusions
400 derived from the PCA based on heavy radiogenic isotopes (§4.4.1). The intrinsic geochemical
401 variation of the depleted upper mantle comforts the image of a marble cake mantle composed
402 of a refractory component and a recycled oceanic crust component. A broad volume of
403 recycled component associated with the high spreading rates in the vicinity of the Chile Ridge
404 Triple junction is therefore a plausible cause of the Pacific Isotopic Bump. The correlation
405 between He and Pb isotopes revealed by our new data (Fig. 6) suggests that the depleted
406 mantle is the outcome of a mixing of a different nature that the one involved in the plume-
407 ridge interaction.
408
409

5. Conclusion

Analyses of this new sampling of the PAR complete the dataset of the Pacific Ridge. Therefore it becomes possible to have a picture of the geochemical variations from 10 to 70°S. Our data show a clear geographical evolution of isotopic characteristics along the Pacific Ridge. In binary isotopic plots, this large-scale variation is expressed by correlations between each isotopic dimension. This observation holds true even for the Nd-Hf system previously reported as decoupled for MORB samples (Debaille et al., 2006). Even more significant in this study is the linear correlation shown in the isotopic He-Nd and $^{3}He/^{4}He$ - $^{206}Pb/^{204}Pb$ plots. In these isotopic spaces, the samples affected by plume-ridge interactions depart clearly from the linear correlations displayed by the ridge samples coming from the depleted mantle.

Despite the paucity of combined Sr-Nd-Pb-Hf isotope data on individual samples, the PCA algorithms used here allow us to portray the variation along a huge section of the Pacific Ridge from a statistical point of view. Compared to previous studies of the sub-Pacific mantle, the application of PCA reveals a Pacific Isotopic Bump, which can be seen as a progressive geochemical variation of the depleted upper-mantle matrix rather than a sharp frontier between two mantle domains. Combining PCA results with the information given by He isotopes, we suggest that the Pacific Isotopic Bump is unrelated to plume-ridge interactions. This geochemical variation in the upper mantle reservoir is the result of a marble-cake mantle assemblage composed of a residual mantle component and a recycled oceanic crust component.

Acknowledgements

The Pb isotope work was funded by CNRS/INSU. The Hf isotope work was supported by NSF grants to B.B. Hanan. We thank Joan Miller for technical assistance at SDSU. We acknowledge Rick Carlson for the editorial handling, Francis Albarède and an anonymous reviewer for constructive comments. Cedric Hamelin thanks the Caltech Tectonic Observatory for its hospitality during his stay in Pasadena. We gratefully acknowledge Neus Sabater for her valuable comments.

References

Agranier, A., Blichert-Toft, J., Graham, D., Debaille, V., Schiano, P., Albarede, F., 2005. The spectra of isotopic heterogeneities along the mid-Atlantic Ridge. Earth Planet. Science Lett., 238(1-2): 96-109.

Albarède, F., 2001. Radiogenic ingrowth in systems with multiple reservoirs: applications to the differentiation of the mantle-crust system. Earth Planet. Science Lett., 189(1-2): 59-73.

Albarède, F., 2008. Rogue mantle Helium and Neon. Science, 319: 943-945.

Allègre, C.J., Staudacher, T., Sarda, P., Kurz, M., 1983. Constraints on evolution of the earth's mantle from rare gas systematic. Nature, 303: 762-766.

Allegre, C.J., Moreira, M., Staudacher, T., 1995. 4He/3He dispersion and mantle convection. Geophysical Research Letters, 22(17): 2325-2328.

Allègre, C.J., 1997. Limitation on the mass exchange between the upper and lower mantle: the evolving convection regime of the Earth. Earth Planet. Science Lett., 150(1-2): 1-6.

Blichert-Toft, J., Albarède, F., 1999. Hf isotopic compositions of the Hawaii Scientific Drilling Project core and the source mineralogy of Hawaiian basalts. Geophys. Res. Lett., 26(7): 935-938.

Blichert-Toft, J., Agranier, A., Andres, M., Kingsley, R., Schilling, J.-G., Albarède, F., 2005. Geochemical segmentation of the Mid-Atlantic Ridge north of Iceland and ridge-hot spot interaction in the North Atlantic. Geochem. Geophys. Geosyst., 6(1): Q01E19.

Cande, S.C., Raymond, C.A., Stock, J. and Haxby, W.F., 1995. Geophysics of the Pitman fracture zone and Pacific-Antarctic plate motions during the Cenozoic. Science, 270: 947-953.

Chauvel, C., Blichert-Toft, J., 2001. A hafnium isotope and trace element perspective on melting of the depleted mantle. Earth Planet. Science Lett., 190(3-4): 137-151.

Class, C., Goldstein, S., 2005. Evolution of helium isotopes in the Earth's mantle. Nature, 436(25): 1107-1112.

Class, C., 2008. Hot arguments to cool off the plume debate? Geology, 36(4): 335-336.

Cooper, K.M., Eiler, J.M., Sims, K.W.W., Langmuir, C.H., 2009. Distribution of recycled crust within the upper mantle: Insights from the oxygen isotope composition of MORB from the Australian-Antarctic Discordance. Geochem. Geophys. Geosyst., 10.

471 Davis, 2010. Noble gases in the dynamic mantle. Geochem. Geophys. Geosyst., 11(3):
472 Q03005.
473 Debaille, V., Blichert-Toft, J., Agranier, A., Doucelance, R., Schiano, P., Albarède, F., 2006.
474 Geochemical component relationships in MORB from the Mid-Atlantic Ridge, 22-
475 35°N. Earth Planet. Science Lett., 241(3-4): 844-862.
476 DePaolo, D.J., Wasserburg, G.J., 1979. Sm-Nd age of the Stillwater complex and the mantle
477 evolution curve for neodymium. Geochim. Cosmochim. Acta, 43: 999-1008.
478 Dosso, L., Bougault, H., Langmuir, C., Bollinger, C., Bonnier, O., Etoubleau, J.,,. (1999). The
479 age and distribution of mantle heterogeneity along the Mid-Atlantic Ridge (31-41°N).
480 Earth Planet. Science Lett., 170: 269-286.
481 Dosso, L., Ondréas, H., Briais, A., Fernagu, P., Floch, G., Hamelin, C., Hanan, B.B.,
482 Klingelhoefer, F., Moreira, M., Normand, A., 2005. The Pacific-Antarctic Ridge
483 between 41°15'S and 52°45'S: Survey and sampling during the PACANTARCTIC 2
484 cruise. InterRidge News, 14: 1-5.
485 Dupré, B., Allègre, C.J., 1983. Pb-Sr isotope variation in Indian Ocean basalts and mixing
486 phenomena. Nature, 303: 142-146.
487 Farley, K.A., Neroda, E., 1998. Noble gases in the Earth's mantle. Annual Review of Earth
488 and Planetary Sciences, 26: 189-218.
489 Gonnermann, H.M., Mukhopadhyay, S., 2009. Preserving noble gases in a convecting mantle.
490 Nature, 459: 560-563.
491 Hamelin, C., Dosso, L., Hanan, B., Barrat, J.-A., Ondréas, H., 2010. Sr-Nd-Hf isotopes along
492 the Pacific Antarctic Ridge from 41 to 53°S. Geophys. Res. Lett., 37(10): L10303.
493 Hanan, B.B., Graham, D.W., 1996. Lead and Helium Isotope Evidence from Oceanic Basalts
494 for a Common Deep Source of Mantle Plumes. Science, 272: 991-995.
495 Hanan, B.B., Blichert Toft, J., Pyle, D.G., Christie, D.M., 2004. Contrasting origins of the
496 upper mantle revealed by hafnium and lead isotopes from the Southeast Indian Ridge.
497 Nature, 432: 91-94.
498 Hart, S.R., 1984. A large scale isotope anomaly in the Southern Hemisphere mantle. Nature,
499 309: 753-757.
500 Hart, S.R., Kurz, M.D., Wang, Z., 2008. Scale length of mantle heterogeneities: Constraints
501 from helium diffusion. Earth Planet. Science Lett., 269(3-4): 508-517.
502 Hémond, C., Hofmann, A.W., Vlastélic, I., Nauret, F., 2006. Origin of MORB enrichment and
503 relative trace element compatibilities along the Mid-Atlantic Ridge between 10° and
504 24°N. Geochem. Geophys. Geosyst., 7, Q12010.

505 Hofmann, A.W., 2003. Sampling mantle heterogeneity through oceanic basalts: Isotopes and
506 trace elements. In: H. Holland and K.K. Turekian (Editors), Treatise on Geochemistry.
507 Elsevier-Pergamon, Oxford, pp. 61-101.
508 Iwamori, H., Albarède, F., 2008. "Decoupled isotopic record of ridge and subduction zone
509 processes in oceanic basalts by independent component analysis." Geochem. Geophys.
510 Geosyst., 9.
511 Iwamori, H., Albarède, F., Nakamura, H., 2010. "Global structure of mantle isotopic
512 heterogeneity and its implications for mantle differentiation and convection." Earth
513 Planet. Science Lett., 299(3-4): 339-351.
514 Ishizuka, O., Taylor, R.N., Milton, J.A., Nesbitt, R.W., 2003. Fluid-mantle interaction in an
515 intra-oceanic arc: constraints from high-precision Pb isotopes. Earth Planet. Science
516 Lett., 211: 221-236.
517 Jackson, M.G., Hart, S.R., Saal, A.E., Shimizu, N., Kurz, M.D., Blusztajn, J.S., Skovgaard,
518 A.C., 2008. Globally elevated titanium, tantalum, and niobium (TITAN) in ocean
519 island basalts with high 3He/4He. Geochem. Geophys. Geosyst., 9(4): 1-21.
520 Jackson, M.G., Kurz, M.D., Hart, S.R., 2009. Helium and neon isotopes in phenocrysts from
521 Samoan lavas: Evidence for heterogeneity in the terrestrial high He-3/He-4 mantle.
522 Earth Planet. Science Lett., 287(3-4): 519-528.
523 Kellogg, J.B., Jacobsen, S.B., O'Connell, R.J., 2007. Modeling lead isotopic heterogeneity in
524 mid-ocean ridge basalts. Earth Planet. Science Lett., 262(3-4): 328-342.
525 Klein, E.M., Langmuir, C.H., Zindler, A., Staudigel, H., Hamelin, B., 1988. Isotope evidence
526 of a mantle convection boundary at the Australian-Antartic discordance. Nature, 333:
527 623-629.
528 Klingelhoefer, F., Ondréas, H., Briais, A., Hamelin, C., Dosso, L., 2006. New structural and
529 geochemical observations from the Pacific-Antarctic Ridge 52°45'S and 41°15'S.
530 Geophys. Res. Lett., 33.
531 Kositsky, A.P., Avouac, J.P., 2010. Inverting geodetic time series with a principal component
532 analysis-based inversion method. J. Geophys. Res., 115(B3): B03401.
533 Kurz, M.D., Jenkins, W.J., Hart, S.R., 1982. Helium isotopic systematics of oceanic islands
534 and mantle heterogeneity. Nature, 297: 43-47.
535 Lonsdale, P., 1994. Geomorphology and structural segmentation of the crest of the southern
536 (Pacific-Antarctic) East Pacific Rise. J. Geophys. Res., 99(B3): 4683-4702.

Meibom, A., Anderson, D.L., Sleep, N.H., Frei, R., Chamberlain, C.P., Hren, M.T., Wooden, J.L., 2003. Are high 3He/4He ratios in oceanic basalts an indicator of deep-mantle plume components? Earth Planet. Science Lett., 208(3-4): 197-204.

Meibom, A., Anderson, D.L., 2004. The statistical upper mantle assemblage. Earth Planet. Science Lett., 217(1-2): 123-139.

Meyzen, C.M., Ludden, J.N., Humler, E., Luais, B., Toplis, M.J., Mével, C., Storey, M., 2005. New insights into the origin and distribution of the DUPAL isotope anomaly in the Indian Ocean mantle from MORB of the Southwest Indian Ridge. Geochem. Geophys. Geosyst., 6(11): 1-34.

Meyzen, C.M., Blichert-Toft, J., Ludden, J.N., Humler, E., Mevel, C., Albarede, F., 2007. Isotopic portrayal of the Earth/'s upper mantle flow field. Nature, 447(7148): 1069-1074.

Moreira, M., Staudacher, T., Sarda, P., Schilling, J.-G., Allègre, C.J., 1995. A primitive plume neon component in MORB: The Shona ridge-anomaly, South Atlantic (51-52°S), Earth Planet. Science Lett., 133, 367-377.

Moreira, M., Dosso, L., Ondréas, H., 2008. Helium isotopes on the Pacific-Antarctic ridge (52.5-41.5°S). Geophys. Res. Lett., 35(L10306): 1-6.

Ondréas, H., Aslanian, D., Géli, L., Olivet, J.-L. and Briais, A., 2001. Variations in axial morphology, segmentation, and seafloor roughness along the Pacific-Antarctic Ridge between 56°S and 66°S. J. Geophys. Res., 106(B5): 8521-8546.

O'Nions, R.K., Peltier, W.R., Davies, J.H., Runcorn, S.K., 1996. Phase-transition modulated mixing in the mantle of the Earth - Discussion. Philosophical Transactions of the Royal Society of London Series A - Mathematical Physical and Engineering Sciences, 354(1711): 1443-1447.

Parman, S.W., Kurz, M.D., Hart, S.R., Grove, T.L., 2005. Helium solubility in olivine and implications for high 3He/4He in ocean island basalts. Nature, 437(7062): 1140-1143.

Patchett, P.J., Tatsumoto, M., 1980. Hafnium isotope variations in oceanic basalts. Geophys. Res. Lett., 7: 1077-1080.

Putirka, K., 2008. Excess temperatures at ocean islands: Implications for mantle layering and convection. Geology, 36(4): 283-286.

Pyle, D.G., Christie, D.M., Mahoney, J.J., 1992. Resolving an isotopic boundary within the Australian-Antarctic Discordance. Earth Planet. Science Lett., 112: 161–178.

569 Rudge, J.F., McKenzie, D., Haynes, P.H., 2005. A theoretical approach to understanding the
570 isotopic heterogeneity of mid-ocean ridge basalt. Geochim. Cosmochim. Acta, 69(15):
571 3873-3887.
572 Salters, V.J.M., White, W.M., 1998. Hf isotope constraints on mantle evolution. Chem. Geol.,
573 145: 447-460.
574 Small, C., Danyushevsky, L.V., 2003. Plate-kinematic explanation for mid-oceanic-ridge
575 depth discontinuities. Geology, 31(5): 399-402.
576 Srebro, N. N., Jaakkola T. 2003, Weighted low-rank approximations, paper presented at 20th
577 International Conference on Machine Learning, Assoc. for the Adv. of Art. Intell.,
578 Washington, D. C.
579 Stracke, A., Bourdon, B., 2009. The importance of melt extraction for tracing mantle
580 heterogeneity. Geochim. Cosmochim. Acta, 73(1): 218-238.
581 Starkey, N.A., Stuart, F.M., Ellam, R.M., Fitton, J.G., Basu, S., Larsen, L.M., 2009. Helium
582 isotopes in early Iceland plume picrites: Constraints on the composition of high He-
583 3/He-4 mantle. Earth Planet. Science Lett., 277(1-2): 91-100.
584 Staudacher, T., Allègre, C.J., 1988. Recycling of oceanic crust and sediments: the noble gas
585 subduction barrier. Earth Planet. Science Lett., 89(2): 173-183.
586 Vlastélic, I., Aslanian, D., Dosso, L., Bougault, H., Olivet, J.L., Géli, L., 1999. Large-scale
587 chemical and thermal division of the Pacific mantle. Nature, 399(6734): 345-350.
588 Vlastélic, I., Dosso, L., Bougault, H., Aslanian, D., Géli, L., Etoubleau, J., Bohn, M., Joron,
589 J.L., Bollinger, C., 2000. Chemical systematics of an intermediate spreading ridge:
590 The Pacific-Antarctic Ridge between 56°S and 66°S. J. Geophys. Res., 105(B2):
591 2915-2936.
592 Vervoort, J.D, Blichert-Toft, J, 1999. Evolution of the depleted mantle: Hf isotope evidence
593 from juvenile rocks through time, Geochim. Cosmochim. Acta, 63, 553-556.
594

Figure captions

Figure 1: Map of the south pacific basin showing the location of the PACANTARCTIC1 and PACANTARCTIC2 cruises with respect to the Pacific Antarctic Ridge (PAR) and the East Pacific Rise (EPR). Hotspot locations are shown in orange on the map.

Figure 2: Examples of binary plots showing correlations within the MORB field. Samples devoid of plume influence are shown in blue whereas samples from plume-ridge interactions are in red. Blue circles represent samples collected along the PAR and blue crosses for EPR samples (all symbols are kept the same in all figures). Mantle reference lines defined in the literature are shown in dashed lines: in the Sr/Nd plot (A), the Pacific Reference Line (PRL) (Vlastélic et al., 1999), in the Nd/Hf plot (B), the mantle array (Vervoort et al., 1999), in the Pb/Pb plot (D), the North Hemisphere Reference Line (NHRL) (Hart, 1984). Since no reference line had yet been recognized in plots involving He isotopes, we show here a regression line ($^3He/^4He = 0.63\ \varepsilon_{Nd} + 1.74$, $r = 0.89$) (C). The projection of the two first principal components (PC1 and PC2) calculated in our study are shown (solid black and grey lines, see text for additional information). Data references can be found in supplementary materials.

Figure 3: Geochemical variations along the PAR and the EPR from 66°S to 10°S. Dashed lines represent the location of major transform faults in the area and a grey shade is used for the Juan Fernandez and Easter Island microplates. The grey curve underlines the large-scale isotopic variation along the pacific ridges from 10 to 66°S and defines the Pacific Isotopic Bump (PIB).

620 **Figure 4:** Plot of the two first principal components along the Pacific Ridge. The similarity
621 between PC2 and δ notation is illustrated by plotting δ(Sr-Pb) as defined by Vlastélic et al.
622 (1999) and Δ^{207}Pb as defined by Hart (1984) versus latitude.
623
624 **Figure 5:** Plot of PC2 versus PC1 for a principal component analysis computed using Sr, Nd,
625 Hf and Pb isotopes. The hashed blue field defines the depleted trend and includes EPR and
626 PAR samples. Data points are drawn as ellipses representing the 95% confidence domain of
627 the components as calculated in Debaille et al. (2006). The insert shows the location of the
628 classical mantle end-members in the PC2 vs PC1 space.
629
630 **Figure 6:** Binary plot of $^{3}He/^{4}He$ vs $^{206}Pb/^{204}Pb$. The dashed regression line ($^{3}He/^{4}He$ = -2.33
631 $^{206}Pb/^{204}Pb$ + 51.0) is defined by samples devoid of plume influence. Plume-ridge interactions
632 (17°S and Easter hotspots) are characterized by positive trends emerging from the PAR-EPR
633 array and pointing towards higher $^{3}He/^{4}He$ (R/Ra) ratios and higher $^{206}Pb/^{204}Pb$.
634
635 **Table 1:** Complete Sr, Nd, Pb, Hf and He isotope data table for PACANTARCTIC 1 and 2
636 samples. In italic font, previously published data (Vlastélic et al., 1999; Vlastélic et al., 2000;
637 Moreira et al., 2008; Hamelin et al., 2010).

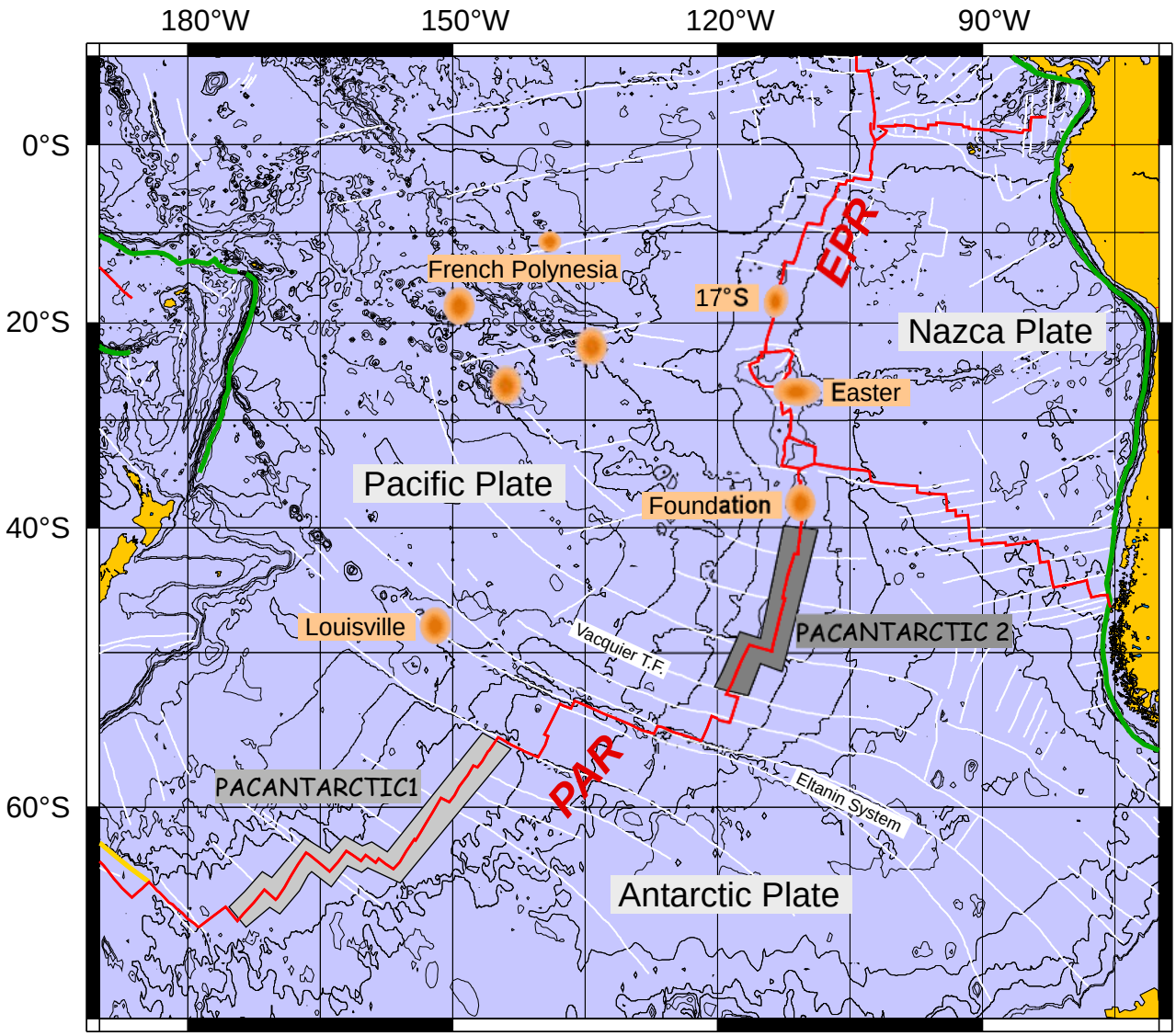
180°W
150°W
120°W
90°W
0°S
20°S
40°S
60°S
French Polynesia
17°S
ERR
Nazca Plate
Easter
Pacific Plate
Foundation
Louisville
Vacquier T.F.
PACANTARCTIC 2
PACANTARCTIC1
PAR
Eltanin System
Antarctic Plate

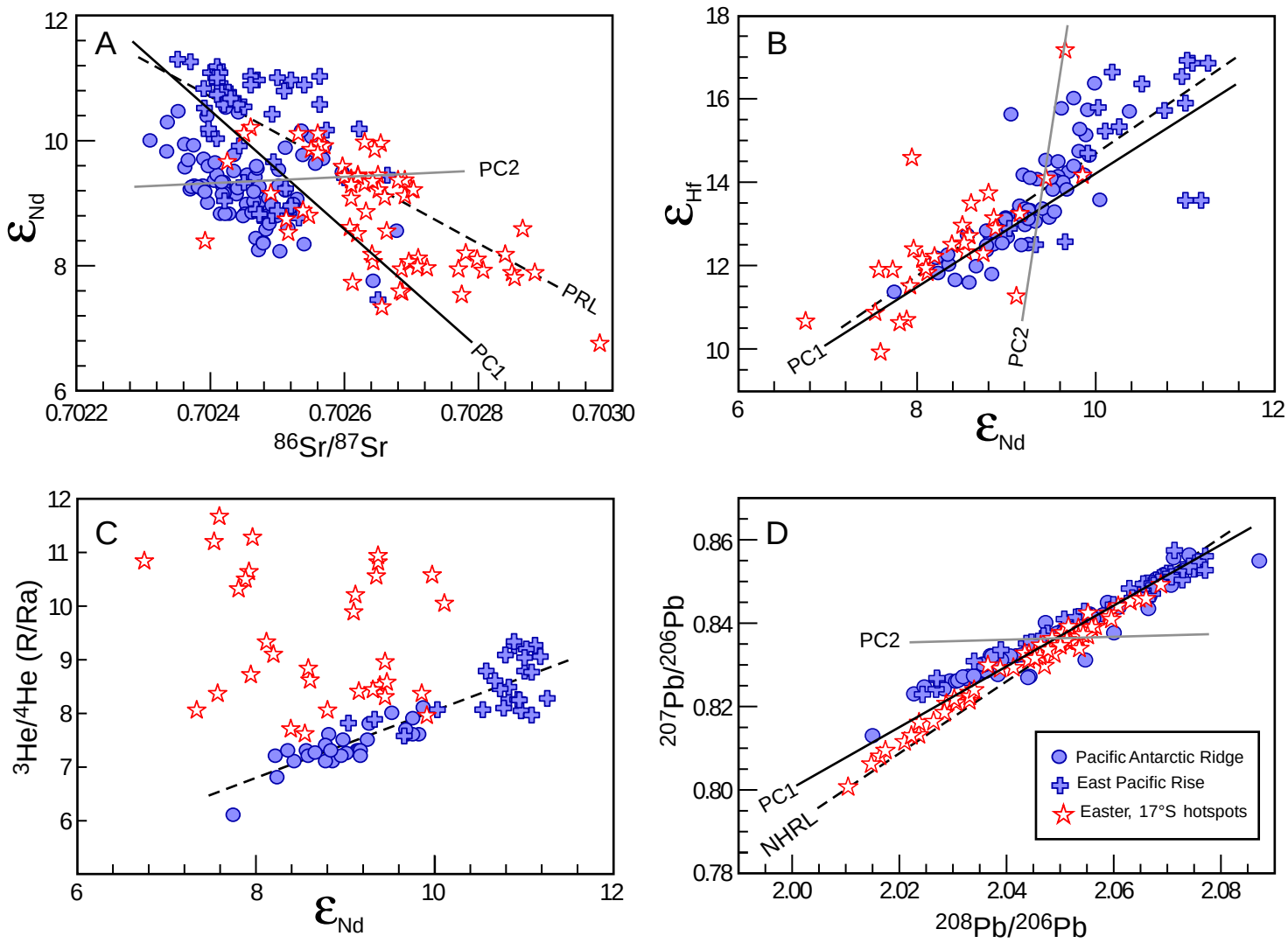
A
B
C
D
PC1
PC2
PRL
NHRL
ε_{Nd}
ε_{Hf}
$^{86}Sr/^{87}Sr$
$^{3}He/^{4}He$ (R/Ra)
$^{207}Pb/^{206}Pb$
$^{208}Pb/^{206}Pb$
Pacific Antarctic Ridge
East Pacific Rise
Easter, 17°S hotspots

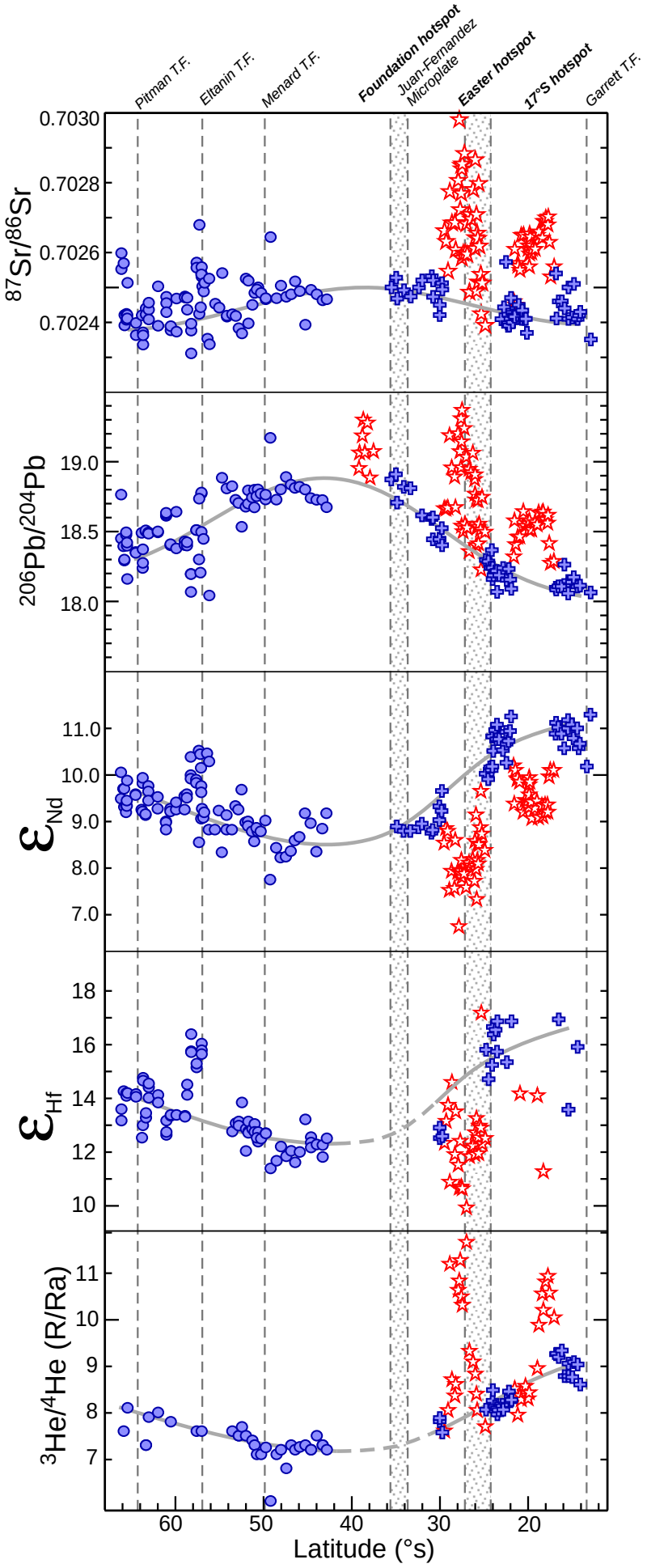
Pitman T.F.
Eltanin T.F.
Menard T.F.
Foundation hotspot
Juan-Fernandez Microplate
Easter hotspot
17°S hotspot
Garrett T.F.
$^{87}Sr/^{86}Sr$
0.7030
0.7028
0.7026
0.7024
$^{206}Pb/^{204}Pb$
19.0
18.5
18.0
ε_{Nd}
11.0
10.0
9.0
8.0
7.0
ε_{Hf}
18
16
14
12
10
$^{3}He/^{4}He$ (R/Ra)
11
10
9
8
7
60
50
40
30
20
Latitude (°s)

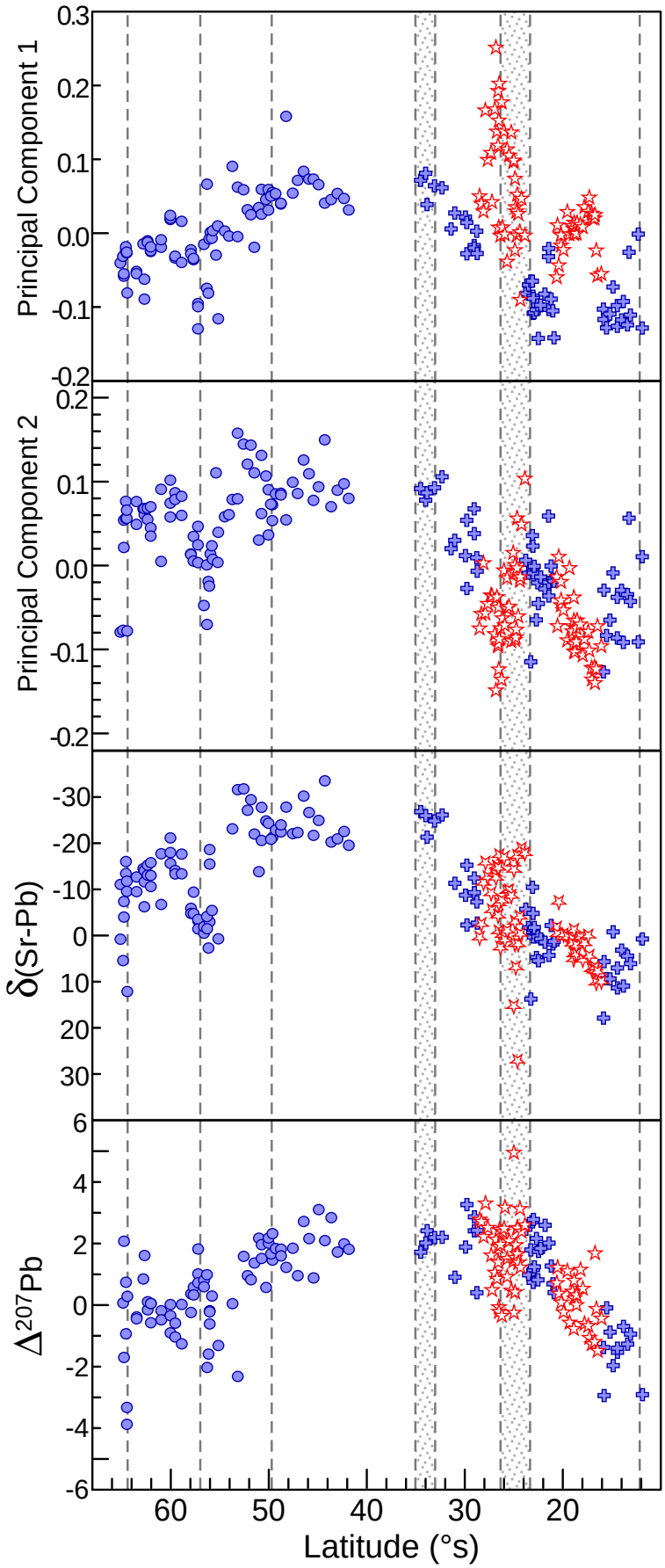
Principal Component 1
0.3
0.2
0.1
0.0
-0.1
-0.2
Principal Component 2
0.2
0.1
0.0
-0.1
-0.2
δ(Sr-Pb)
-30
-20
-10
0
10
20
30
Δ207Pb
6
4
2
0
-2
-4
-6
60
50
40
30
20
Latitude (°s)

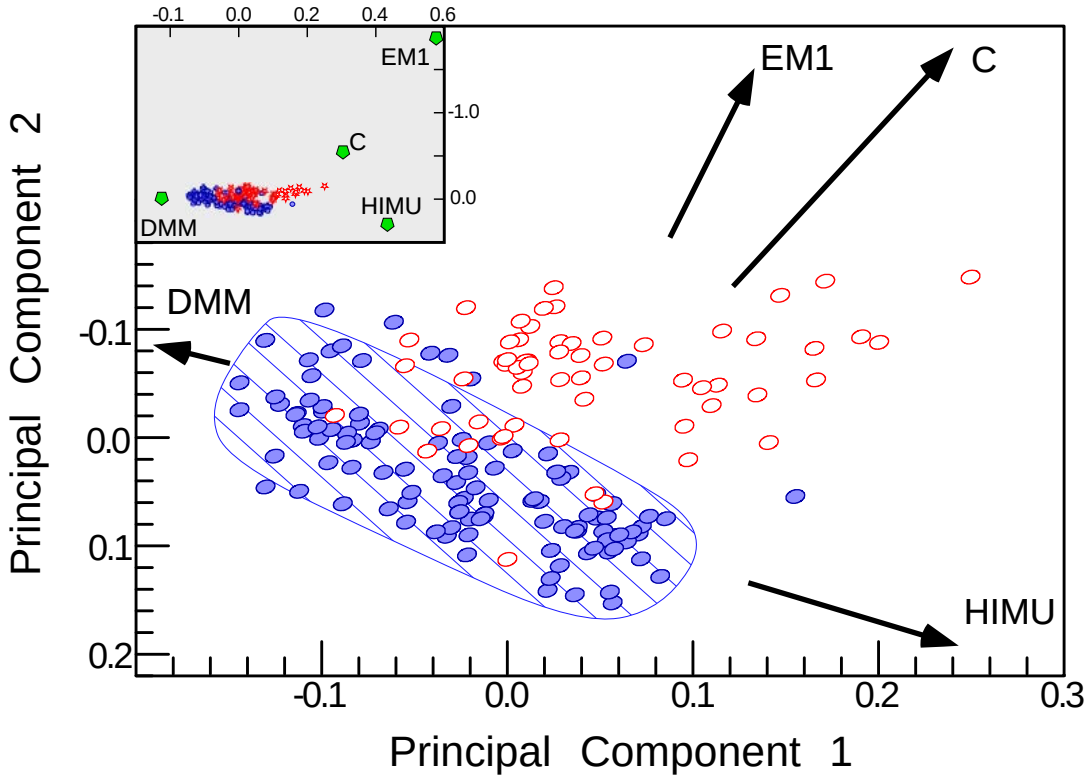
-0.1
0.0
0.2
0.4
0.6
EM1
C
HIMU
DMM
-1.0
0.0
EM1
C
DMM
HIMU
-0.1
0.0
0.1
0.2
0.3
Principal Component 2
Principal Component 1

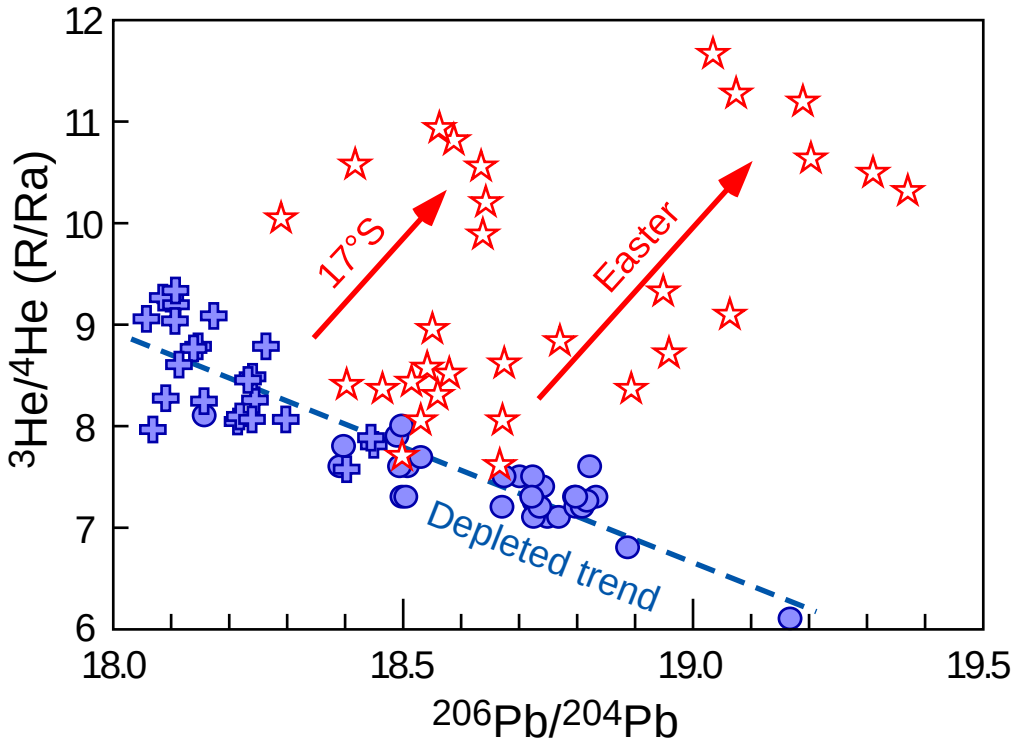
12
11
10
9
8
7
6
18.0
18.5
19.0
19.5
$^{3}He/^{4}He$ (R/Ra)
$^{206}Pb/^{204}Pb$
17°S
Easter
Depleted trend

Table 1: Complete Sr, Nd, Pb, Hf and He isotope data table for PACANTARCTIC 1 and 2 samples. In italic font, previously published data (Vlastélic et al., 1999; Vlastélic et al., 2000; Moreira et al., 2008; Hamelin et al., 2010).

	$^{87}Sr/^{86}Sr$	$^{143}Nd/^{144}Nd$	ε_{Nd}	$^{206}Pb/^{204}Pb$	$^{207}Pb/^{204}Pb$	$^{208}Pb/^{204}Pb$	$^{176}Hf/^{177}Hf$	ε_{Hf}	$^{3}He/^{4}He$	Long. (°)	Lat. (°)	Depth
PACANTARCTIC 2												
PAC2DR38-1	*0.702465*	*0.513108*	*9.17*	18.671	15.533	38.039	*0.283125*	*12.50*	*7.2*	-111.3	-41.80	2524
PAC2DR37-1	*0.702462*	*0.513091*	*8.84*	18.722	15.540	38.110	*0.283106*	*11.80*	*7.3*	-111.3	-42.27	2475
PAC2DR37-2							*0.283118*	*12.25*	*7.3*	-111.3	-42.27	2475
PAC2DR36-1	*0.702479*	*0.513066*	*8.34*	18.724	15.538	38.117	*0.283119*	*12.27*	*7.5*	-111.6	-42.95	2503
PAC2DR35-1a							*0.283121*	*12.34*	*7.2*	-111.8	-43.59	2463
PAC2DR35-2	*0.702492*	*0.513097*	*8.95*	18.736	15.550	38.146	*0.283127*	*12.54*	*7.2*	-111.8	-43.59	2463
PAC2DR34-1	*0.702392*	*0.513108*	*9.17*	18.798	15.549	38.234	*0.283145*	*13.20*	*7.3*	-112.0	-44.24	2467
PAC2DR33-1	*0.702488*	*0.513082*	*8.66*	18.817	15.562	38.236	*0.283111*	*11.99*	*7.26*	-112.3	-44.87	2374
PAC2DR32-1	*0.702516*	*0.513078*	*8.58*	18.809	15.539	38.202	*0.283100*	*11.60*	*7.2*	-112.4	-45.39	2384
PAC2DR31-3	*0.702479*	*0.513066*	*8.36*	18.833	15.554	38.242	*0.283112*	*12.03*	*7.3*	-112.7	-45.85	2414
PAC2DR30-1	*0.702472*	*0.513060*	*8.24*	18.887	15.565	38.311	*0.283106*	*11.83*	*6.8*	-112.9	-46.40	2345
PAC2DR29-1	*0.702504*	*0.513059*	*8.22*	18.798	15.538	38.208	*0.283117*	*12.19*	*7.2*	-113.1	-47.01	2407
PAC2DR28-2	*0.702468*	*0.513070*	*8.43*	18.725	15.539	38.121	*0.283102*	*11.66*	*7.1*	-113.3	-47.51	2489
PAC2DR27-1	*0.702643*	*0.513035*	*7.74*	19.168	15.581	38.624	*0.283094*	*11.37*	*6.1*	-113.4	-48.18	2359
PAC2DR22-1	*0.702465*	*0.513100*	*9.01*	18.726	15.539	38.153	*0.283131*	*12.69*	*7.25*	-113.6	-48.73	2413
PAC2DR22-3	*0.702468*			18.761	15.540	38.202	*0.283130*	*12.68*		-113.6	-48.73	2413
PAC2DR21-2	*0.702483*	*0.513088*	*8.78*	18.768	15.544	38.189	*0.283125*	*12.48*	*7.1*	-113.8	-49.26	2339
PAC2DR9-1	*0.702499*	*0.513088*	*8.78*	18.768	15.540	38.202	*0.283122*	*12.37*		-117.0	-49.59	2380
PAC2DR9-2				18.798	15.552	38.244	*0.283132*	*12.73*		-117.0	-49.59	2380
PAC2DR20-1	*0.702493*	*0.513092*	*8.86*	18.749	15.540	38.168	*0.283126*	*12.51*	*7.1*	-116.8	-49.73	2441
PAC2DR8-1	*0.702483*	*0.513077*	*8.56*	18.796	15.550	38.237	*0.283132*	*12.74*	*7.3*	-117.1	-49.99	2221
PAC2DR8-2				18.670	15.535	38.031	*0.283140*	*13.03*		-117.1	-49.99	2221
PAC2DR7-4	*0.702449*	*0.513088*	*8.78*	18.741	15.528	38.148	*0.283135*	*12.84*	*7.4*	-117.2	-50.25	2229
PAC2DR6-1	*0.702518*	*0.513094*	*8.90*	18.792	15.543	38.201	*0.283133*	*12.75*		-117.2	-50.70	2610
PAC2DR6-6	*0.702396*	*0.513099*	*8.99*	18.696	15.537	38.123	*0.283143*	*13.12*		-117.2	-50.70	2610
PAC2DR5-2g	*0.702524*	*0.513098*	*8.97*	18.674	15.537	38.110	*0.283135*	*12.85*	*7.5*	-117.4	-50.98	2784
PAC2DR4-2	*0.702367*	*0.513134*	*9.68*	18.531	15.513	37.942	*0.283163*	*13.83*	*7.7*	-117.8	-51.43	2409
PAC2DR3-1							*0.283139*	*12.97*	*7.5*	-118.0	-51.79	2397
PAC2DR3-3	*0.702382*	*0.513112*	*9.25*	18.701	15.526	38.092	*0.283143*	*13.12*	*7.5*	-118.0	-51.79	2397
PAC2DR2	*0.702417*	*0.513116*	*9.32*	18.724	15.530	38.110	*0.283141*	*13.06*		-118.1	-52.13	2405
PAC2DR1-1	*0.702422*	*0.513090*	*8.81*	18.822	15.547	38.199	*0.283133*	*12.75*	*7.6*	-118.4	-52.53	2323
PACANTARCTIC 1												
PAC1DR14-2	*0.702538*	*0.513138*	*9.75*	18.494	15.489	38.100	0.283225	16.02	7.6	-145.09	-56.00	2617
PAC1DR14-3	*0.702530*	*0.513102*	*9.05*	18.776	15.524	38.379	0.283214	15.63		-145.09	-56.00	2617
PAC1DR14-4	*0.702557*	*0.513131*	*9.62*	18.769	15.523	38.370	0.283218	15.77		-145.09	-56.00	2617
PAC1DR13-2g	*0.702556*	*0.513142*	*9.82*	18.508	15.503	37.954	0.283204	15.28	7.6	-145.74	-56.57	2674
PAC1DR13-3	*0.702570*	*0.513145*	*9.89*	18.508	15.505	37.963	0.283200	15.14		-145.74	-56.57	2674
PAC1DR12-1g	*0.702310*	*0.513150*	*9.99*	18.064	15.467	37.468	0.283235	16.37		-146.29	-57.18	2539
PAC1DR12-3g	*0.702375*	*0.513146*	*9.91*	18.194	15.473	37.627	0.283217	15.74		-146.29	-57.18	2539
PAC1DR12-3r	*0.702395*	*0.513170*	*10.38*	18.192	15.470	37.620	0.283216	15.70		-146.29	-57.18	2539
PAC1DR11-1g	*0.702435*	*0.513125*	*9.50*	18.420	15.491	37.877	0.283171	14.11		-146.80	-57.63	2500
PAC1DR11-3	*0.702469*	*0.513129*	*9.58*	18.397	15.491	37.816	0.283182	14.50		-146.80	-57.63	2500
PAC1DR10-1g	*0.702473*	*0.513112*	*9.25*	18.426	15.492	37.881	0.283149	13.33		-148.50	-57.89	2319
PAC1DR10-3	*0.702470*	*0.513127*	*9.54*	18.400	15.483	37.798	0.283148	13.30		-148.50	-57.89	2319
PAC1DR09-g	*0.702467*	*0.513120*	*9.40*	18.638	15.511	38.075	0.283150	13.37		-149.14	-58.85	2484
PAC1DR09-1	*0.702372*	*0.513112*	*9.25*	18.376	15.470	37.819				-149.14	-58.85	2484
PAC1DR08-2	*0.702388*	*0.513110*	*9.21*	18.406	15.480	37.827	0.283150	13.37		-150.02	-59.5	2365
PAC1DR08-3	*0.702376*	*0.513113*	*9.27*	18.398	15.475	37.809	0.283149	13.33	7.8	-150.02	-59.5	2365
PAC1DR07-1g	*0.702472*	*0.513099*	*8.99*	18.609	15.505	38.039	0.283144	13.16		-152.08	-60.00	2362
PAC1DR07-2g	*0.702454*	*0.513098*	*8.97*	18.620	15.509	38.062	0.283129	12.63		-152.08	-60.00	2362
PAC1DR07-3	*0.702428*	*0.513090*	*8.82*	18.631	15.501	38.041	0.283132	12.73		-152.08	-60.00	2362
PAC1DR06-g	*0.702502*	*0.513126*	*9.52*	18.498	15.491	37.911	0.283163	13.83	8	-153.21	-60.94	2527
PAC1DR06-2	*0.702389*	*0.513113*	*9.27*	18.491	15.493	37.912	0.283171	14.11		-153.21	-60.94	2527
PAC1DR05-1g	*0.702407*	*0.513132*	*9.64*	18.489	15.495	37.926	0.283168	14,00		-154.54	-62.00	2344
PAC1DR05-3	*0.702435*	*0.513138*	*9.75*	18.490	15.496	37.936	0.283179	14.39	7.9	-154.54	-62.00	2344
PAC1DR05-r	*0.702455*	*0.513122*	*9.44*	18.482	15.488	37.904	0.283183	14.53		-154.54	-62.00	2344
PAC1DR03-1	*0.702421*	*0.513107*	*9.15*	18.505	15.498	37.974	0.283152	13.44	7.3	-156.08	-62.32	2219
PAC1DR03-2	*0.702439*	*0.513106*	*9.13*	18.498	15.494	37.965	0.283147	13.26	7.3	-156.08	-62.32	2219
PAC1DR02-g	*0.702335*	*0.513141*	*9.81*	18.272	15.511	37.837	0.283189	14.75		-156.54	-62.64	2489
PAC1DR02-1	*0.702362*	*0.513147*	*9.93*	18.369	15.498	37.860	0.283186	14.64		-156.54	-62.64	2489
PAC1CV09	*0.702370*	*0.513110*	*9.21*	18.236	15.588	38.063	0.283139	12.98		-159.61	-62.66	2714
PAC1CV08	*0.702419*	*0.513112*	*9.25*	18.487	15.503	37.965	0.283126	12.52		-162.44	-62.77	2534
PAC1CV06-r	*0.702362*	*0.513128*	*9.56*	18.344	15.475	37.787	0.283169	14.04		-166.06	-63.45	2755
PAC1CV06-g	*0.702397*	*0.513129*	*9.58*	18.350	15.476	37.804	0.283172	14.15		-166.06	-63.45	2755
PAC1CV04-g	*0.702512*	*0.513144*	*9.87*	18.157	15.462	37.575	0.283173	14.18	8.1	-169.40	-64.4	2340
PAC1CV03-r	*0.702423*	*0.513109*	*9.19*	18.475	15.501	37.952	0.283173	14.18		-171.88	-64.53	2576
PAC1CV03-g	*0.702406*	*0.513117*	*9.34*	18.492	15.486	37.923	0.283170	14.07		-171.88	-64.53	2576
PAC1CV02-g	*0.702568*	*0.513135*	*9.69*	18.391	15.485	37.868	0.283175	14.25	7.6	-172.43	-64.83	2936
PAC1CV01-r	*0.702551*	*0.513153*	*10.05*	18.447	15.557	38.121	0.283156	13.58		-173.75	-65.10	2863
PAC1CV01-g	*0.702597*	*0.513124*	*9.48*	18.761	15.591	38.549	0.283144	13.16		-173.75	-65.10	2863

Supplementary Material

New algorithm to compute a PCA:

The PCA method is a linear transformation that converts the data into a new coordinate system in which the direction along which the greatest data variance is expressed, becomes the first axis (PC1). The direction along which the greatest data variance is expressed orthogonal to PC1 becomes the second axis (PC2), and so on. The first step, called the whitening, consists in normalizing the data. This is done by subtracting the mean value from each data point and dividing the result by the standard deviation of each variable. The correlation matrix (Pearson's correlation matrix) of the reduced variables can then be calculated. The next step consists into diagonalizing the correlation matrix in order to find the eigenvalues, which correspond to the dimensions that have the strongest correlation in the data set. The principal components are the coordinates of the data points in the eigenvector referential.

The PCA method used with our geochemical dataset has been initially developed for low-rank matrix approximations (Srebro and Jaakkola, 2003) and was recently adapted for tectonic problems using incomplete geodetic times series (Kositsky and Avouac, 2010). The algorithm used to compute our principal components has been written specifically to address the major problem of a geochemical database: missing data in the matrix. Traditionally, for a given sample, it is necessary to acquire as many different isotope measurements as the number of dimensions used in the PCA. The paucity of combined Sr-Nd-Pb-Hf isotope data in individual samples is therefore an important issue for standard PCA algorithms. The more dimensions we use in the PCA, the fewer samples meet the required conditions: from 210 samples for 2-dimension (Sr-Nd) space to only 99 samples for a 6-dimension space. The main difference with a classical PCA is that we have replaced the standard Singular Value Decomposition (SVD) with a more sophisticated decomposition proposed by Srebro and Jaakkola [2003]. In this approach the data matrix X is decomposed into components U, S, V, with each data point weighted according to the square of its standard error. This decomposition is particularly adapted to take into account individual measurement errors and deal with missing data points. It allows us to compute the Principal Components on the entire data set, even if some isotopic ratios are missing. Each missing data point is weighted with infinite standard error. We want to emphasize that, consequently, no interpolation is made, which could erase some local effect. This technique is particularly suitable to geochemical data as it allows us to complete the principal components using the whole dataset, increasing therefore the accuracy of the calculation.

Limits of PCA:

Classical limits related to PCA calculation:

Because the PCA method is an orthogonal linear transformation, it assumes the linearity of the data co-variations. In most binary isotopic diagrams, mixing processes are expressed by hyperboles whose curvatures depend on the elemental concentration ratios of the involved end-members. But in the case of MORB, pseudo-linear correlations are observed (Fig. 2) indicating that denominator elements are in approximately constant proportions in the mixing components. It is very difficult to evaluate the extent of non-linear relationships concealed within the analytical noise. However, it is interesting to note that the geographical variations of the components calculated with our method are approximately the same as those computed in the 3-dimensional space of Pb isotopes, in which relationships are linear. In order to minimize the correlations induced by the ^{204}Pb analytical noise (it represents only about 1.4% of the total Pb), the computation has been made in the ^{204}Pb/^{206}Pb, ^{207}Pb/ ^{206}Pb and ^{208}Pb/ ^{206}Pb space. Considering the problematic of our study, this observation suggests that the curvature can be neglected.

Limits related to our new algorithm:

Compared to traditional PCA algorithms, principal components are computed here altogether rather than separately, because the number of components affects the subspace in which these components reside. A limit to this method appears if one variable is represented by fewer samples than compared to other variables. In this particular case, a sample with a value corresponding to this “rare” variable is artificially given more weight. In return, each variable is also weighed in proportion to its number of samples. Because the number of He isotope analyses along the studied ridge section is too low compared to other isotopes, the information provided by this parameter has not been included in the PCA calculation.

Distribution of the variance among the principal components:

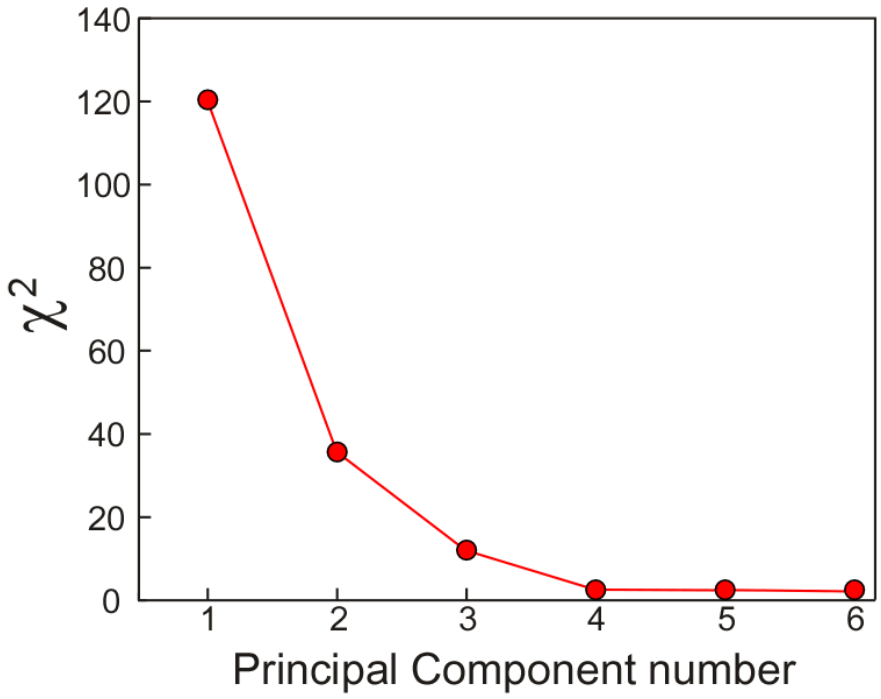

Plot of the residual variance (χ^2) versus the principal component number

Figure 2 data references:

Bach, W., Hegner, E., Erzinger, J., Satir, M., 1994. Chemical and isotopic variations along the superfast spreading East Pacific Rise from 6° S to 30° S. Contribution to Mineralogy and Petrology, 116(4): 365-380.

Castillo, P., 1988. The Dupal anomaly as a trace of the upwelling lower mantle. Nature, 336: 667-670.

Fontignie, D., Schilling, J.-G., 1991. 87Sr/86Sr and REE variations along the Easter Microplate boundaries (south Pacific): Application of multivariate statistical analyses to ridge segmentation. Chemical Geology, 89: 209-241.

Hanan, B.B., 1989. Easter Microplate evolution: Pb isotope evidence, Journal Geophysical Research, 94: 7432-7448.

Kingsley, R.H., Blichert-Toft, J., Fontignie, D., Schilling, J.G., 2007. Hafnium, neodymium, and strontium isotope and parent-daughter element systematics in basalts from the plume-ridge

interaction system of the Salas y Gomez Seamount Chain and Easter Microplate. Geochem Geophys Geosyst, 8: 28.

Kurz, M.D., Moreira, M., Curtice, J., Lott Iii, D.E., Mahoney, J.J., Sinton, J.M., 2005. Correlated helium, neon, and melt production on the super-fast spreading East Pacific Rise near 17°S. Earth Planet. Sci. Lett., 232(1-2): 125-142.

Mahoney, J.J., Sinton, J.M., Kurz, M.D., Macdougall, J.D, Spencer, K.J., Lugmair, G.W., 1994. Isotope and trace element characteristics of a super-fast spreading ridge: East Pacific Rise 13-23°S. Earth Planet. Sci. Lett., 121: 173-193.

Maia, M., C. Hemond and P. Gente 2001. Contrasted interactions between plume, upper mantle, and lithosphere: Foundation chain case. Geochem Geophys Geosyst 2: U25-U53.

Niu, Y.L., Waggoner, D.G., Sinton, J.M., Mahoney, J.J., 1996. Mantle source heterogeneity and melting processes beneath seafloor spreading centers: The East Pacific Rise, 18 degrees-19S. Journal of Geophysical Research, 101(B12): 27711-27733.

Nowell, G.M., Kempton, P.D., Noble, S.R., Fitton, J.G., Saunders, A.D., Mahoney, J.J., Taylor, R.N., 1998. High precision Hf isotope measurements of MORB and OIB by thermal ionisation mass spectrometry: insights into the depleted mantle. Chemical Geology, 149(3-4): 211-233.

Vlastélic, I., Dosso, L., Guillou, H., Bougault, H., Geli, L., Etoubleau, J., Joron, J.L., 1998. Geochemistry of the Hollister Ridge: relation with the Louisville hotspot and the Pacific-Antarctic Ridge. Earth Planet. Sci. Lett., 160(3-4): 777-793.

White, W.M., Hofmann, A.W., Puchelt, H., 1987. Isotope geochemistry of Pacific mid-ocean ridge, Journal Geophysical Research, 92: 4881-4893.